

Failure of thymic deletion and instability of autoreactive Tregs drive autoimmunity in immune-privileged liver

Max Preti, Lena Schlott, David Lübbing, Daria Krzikalla, Anna-Lena Müller, Fenja A. Schuran, Tobias Poch, Miriam Schakat, Sören Weidemann, Ansgar W. Lohse, Christina Weiler-Normann, Marcial Sebode, Dorothee Schwinge, Christoph Schramm, Antonella Carambia, Johannes Herkel

JCI Insight. 2021. <https://doi.org/10.1172/jci.insight.141462>.

Research **In-Press Preview** **Hepatology**

The liver is an immune-privileged organ that can deactivate autoreactive T cells. Yet in autoimmune hepatitis (AIH), autoreactive T cells can defy hepatic control and attack the liver. To elucidate how tolerance to self-antigens is lost during AIH pathogenesis, we generated a spontaneous mouse model of AIH, based on recognition of an MHC class II-restricted model peptide in hepatocytes by autoreactive CD4 T cells. We find that the hepatic peptide was not expressed in the thymus leading to deficient thymic deletion and resulting in peripheral abundance of autoreactive CD4 T cells. In the liver, autoreactive CD4 effector T cells accumulated within portal ectopic lymphoid structures and matured towards pathogenic IFNy and TNF co-producing cells. Expansion and pathogenic maturation of autoreactive effector T cells was enabled by a selective increase of plasticity and instability of autoantigen-specific Tregs, but not of non-specific Tregs. Indeed, antigen-specific Tregs were reduced in frequency and manifested increased IL-17 production, reduced epigenetic demethylation and reduced expression of *Foxp3*. As a consequence, autoantigen-specific Tregs had a reduced suppressive capacity, as compared to non-specific Tregs. In conclusion, loss of tolerance and the pathogenesis of AIH were enabled by combined failure of thymic deletion and peripheral regulation.

Find the latest version:

<https://jci.me/141462/pdf>



Failure of thymic deletion and instability of autoreactive Tregs drive autoimmunity in immune-privileged liver

Max Preti¹, Lena Schlott¹, David Lübbingering¹, Daria Krzikalla¹, Anna-Lena Müller¹, Fenja A. Schuran¹, Tobias Poch¹, Miriam Schakat¹, Sören Weidemann², Ansgar W. Lohse¹, Christina Weiler-Normann¹, Marcial Sebode¹, Dorothee Schwinge¹, Christoph Schramm^{1,3}, Antonella Carambia^{1*}, Johannes Herkel^{1*}

¹ Department of Medicine I, University Medical Centre Hamburg-Eppendorf, Hamburg, Germany

² Department of Pathology, University Medical Centre Hamburg-Eppendorf, Hamburg, Germany

³ Martin Zeitz Center for Rare Diseases, University Medical Centre Hamburg-Eppendorf, Hamburg, Germany

* equal contribution

Correspondence:

Antonella Carambia or Johannes Herkel

Department of Medicine I, University Medical Centre Hamburg-Eppendorf
Martinistr. 52. 20246 Hamburg, Germany

Phone: (+49) 40 7410 59736; Fax: (+49) 40 7410 58014

a.carambia@uke.de or jherkel@uke.de

Conflict of interest statement

The authors have declared that no conflict of interest exists.

Abstract

The liver is an immune-privileged organ that can deactivate autoreactive T cells. Yet in autoimmune hepatitis (AIH), autoreactive T cells can defy hepatic control and attack the liver. To elucidate how tolerance to self-antigens is lost during AIH pathogenesis, we generated a spontaneous mouse model of AIH, based on recognition of an MHC class II-restricted model peptide in hepatocytes by autoreactive CD4 T cells. We find that the hepatic peptide was not expressed in the thymus leading to deficient thymic deletion and resulting in peripheral abundance of autoreactive CD4 T cells. In the liver, autoreactive CD4 effector T cells accumulated within portal ectopic lymphoid structures and matured towards pathogenic IFN γ and TNF co-producing cells. Expansion and pathogenic maturation of autoreactive effector T cells was enabled by a selective increase of plasticity and instability of autoantigen-specific Tregs, but not of non-specific Tregs. Indeed, antigen-specific Tregs were reduced in frequency and manifested increased IL-17 production, reduced epigenetic demethylation and reduced expression of *Foxp3*. As a consequence, autoantigen-specific Tregs had a reduced suppressive capacity, as compared to non-specific Tregs. In conclusion, loss of tolerance and the pathogenesis of AIH were enabled by combined failure of thymic deletion and peripheral regulation.

Introduction

Autoimmune diseases are caused by a tissue-damaging immune response of lymphocytes recognizing self-antigens (1). The clinical conditions caused by autoimmunity often impose severe health burdens on affected individuals, and collectively represent a major economic burden for healthcare systems (1). Although many autoreactive T cells are efficiently deleted at an immature state in the thymus, it has been demonstrated that self-reactive T cells are a constitutive part of the mature lymphocyte repertoire in healthy individuals (2, 3, 4). Nonetheless, the activation of these mature autoreactive T cells seems to be tightly controlled by various mechanisms, first and foremost by regulatory T cells (Tregs) (4, 5, 6). Hence, autoreactive T cell activation rarely produces more than subclinical, self-limited autoimmune episodes in most subjects. The reasons why some individuals develop self-sustained autoimmune diseases despite these regulatory mechanisms are not clear.

A particular challenge is to conceptualise those autoimmune diseases that affect immune-privileged organs such as the liver, which actually has a distinct capacity to induce immune tolerance (7,8). Indeed, the liver can even protect other organs from immune-mediated damage, as has been demonstrated by co-transplantation of skin and liver allografts (9), or by complete protection from autoimmune neuroinflammation induced by genetic or nanoparticle-mediated transfer of neuroantigens to liver cells (10, 11). Given this potent tolerance-inducing capacity of the liver, it is surprising that the liver cannot protect itself from autoimmune attack in autoimmune liver diseases, such as autoimmune hepatitis (AIH).

AIH is a chronic inflammatory liver disease that can occur in all ages and ethnicities, with heterogeneous clinical manifestations ranging from inconspicuous presentation up to fulminant liver failure (12). Typical disease features include elevated serum transaminases, elevated IgG or gamma globulins, the presence of autoantibodies, such as anti-nuclear antibodies (ANA), and a histological picture of interface hepatitis with mainly lymphocytic infiltrates (12). Thus far, the aetiology and pathogenesis of AIH are unclear, but it is assumed that AIH is driven by an adaptive immune response to hepatocellular autoantigens (12). Indeed, several antigen-driven AIH mouse models have demonstrated that T cell responses

to liver antigens can cause liver inflammation (13-19). Nonetheless, the mechanisms that produce the loss of tolerance to liver antigens in AIH are not fully understood. A drawback of the available mouse models is the difficulty to characterise and distinguish autoantigen-specific from non-specific T cells. Moreover, the majority of the available AIH mouse models require extrinsic provision of strong immune activators to overcome hepatic tolerance (13, 19), which might not reflect the natural disease development.

It is now recognized that the potent immune activation in autoimmune diseases often occurs within ectopic (or tertiary) lymphoid tissue (ELT) that develop in the target organs of autoimmunity (20). ELTs are ordered structures induced within affected organs that resemble the organization of lymphoid follicles in secondary lymphatic organs, frequently displaying segregated T cell and B cell zones, presence of dendritic cells (DCs) and high endothelial venules (21). In several chronic inflammatory liver diseases, ELTs can be found mostly within portal fields (22, 23). However, little is known about a possible role of ELTs in AIH pathogenesis.

Besides being driven by strong activation of effector T cells, AIH might also be associated with reduced functionality of regulatory T cells (Tregs). Tregs are critical mediators of self-tolerance and their loss or dysfunction can lead to autoimmune disease (6), and several observations (reviewed in 24, 25) suggest that Tregs have the potential to modulate AIH. However, their precise role in AIH pathogenesis is unclear, as contradictory findings with respect to their overall frequency and functionality have been reported (26,27). Intriguingly, hepatic infiltrates in AIH reportedly contain Tregs (27, 28, 29), suggesting that the inflammatory environment in AIH livers may override the suppressive capacity of the hepatic Tregs (30, 31). Indeed, Tregs can display considerable plasticity that allows for adaptation to various physiological conditions (32, 33); however, in the context of autoimmune liver inflammation, this plasticity might result in impaired function.

To further explore the mechanisms underlying the loss of tolerance to liver antigens in AIH, we here investigate a new mouse model that is characterized by hepatocellular expression of an MHC class II-restricted immunodominant T cell epitope of the lymphocytic

choriomeningitis virus (GP61-80), and by abundance of cognate CD4 T cells recognizing GP61-80 expressed by hepatocytes. These mice spontaneously developed CD4 T cell-mediated autoimmune hepatitis with typical disease features of human AIH. We demonstrate that AIH is driven by escape from thymic deletion and hepatic activation of CD4 effector T cells, which was fostered by selective failure of peripherally induced autoreactive Tregs.

Results

Absent thymic deletion of CD4 T cells recognizing a liver-restricted peptide

We constructed a mutated invariant chain molecule (CD74) in which the CLIP peptide sequence was replaced by the LCMV GP61-80 peptide sequence, and inserted the mutated gene flanked by loxP sites into the *Rosa26* gene, as has been done before with a similar construct (34) (Figure 1A). These mice with inducible GP expression (iGP) were bred with Smarta mice that are transgenic for the Smarta1 T cell receptor recognizing the GP61-80 peptide (35). Conditional expression in hepatocytes was subsequently achieved by breeding with Alb-Cre mice; as control, conditional expression in dendritic cells was achieved by breeding with Itgax-Cre mice (Figure 1B). The resulting Alb-iGP_Smartas and Itgax-iGP_Smartas mice were analysed by quantitative RT-PCR for expression of the recombinant GP peptide in the thymus and in the liver (Figure 1C). As expected, GP expression was low in Itgax-iGP_Smartas livers and high in Alb-iGP_Smartas livers (0.10 vs. 2.59; $p=0.0159$). In contrast, GP expression was high in Itgax-iGP_Smartas thymi and virtually absent in Alb-iGP_Smartas thymi (0.87 vs. 0.039; $p=0.0159$). We then analysed Itgax-iGP_Smartas and Alb-iGP_Smartas mice for deletional tolerance mechanisms, using I-A(b) LCMV GP 66-77 tetramers that specifically stain those T cells recognizing the GP peptide (Figure 1D). We found that virtually all GP-reactive T cells were subjected to thymic deletion in Itgax-iGP_Smartas mice (Figure 1E; 0.68%; $p<0.0001$). Accordingly, GP-reactive CD4 T cells were negligible in the spleen of Itgax-iGP_Smartas mice (0.85%; $p<0.0001$). In contrast, there was almost no deletion of GP-reactive Smarta cells in the thymus of Alb-iGP_Smartas mice, which had a similar frequency of antigen-specific cells as Smarta control mice that do not express the cognate GP peptide (Figure 1E; 85.3% vs. 80.6%; $p=0.8414$). Accordingly, only a moderate reduction of GP-reactive CD4 T cells was found in the spleen of Alb-iGP_Smartas mice (73.2% vs. 92.7% in Smarta mice; $p<0.0001$). Thus, the GP61-80 peptide did not seem to trigger extensive deletion of the specific CD4 Smarta cells in Alb-iGP_Smartas mice, neither in the thymus nor in the periphery.

Spontaneous autoimmune hepatitis in mice featuring autoantigen peptide in the liver and peripheral autoreactive T cells

To address whether the conditional expression of GP in hepatocytes and the presence of GP-specific Smarta cells resulted in autoimmune disease, we monitored Alb-iGP_Smartas mice over time, and, as control, Itgax-iGP_Smartas mice and Alb-iGP mice that both lacked GP-specific Smarta cells. Whereas Itgax-iGP_Smartas and Alb-iGP mice remained healthy over an observation period of one year, Alb-iGP_Smartas mice that were replete with GP-reactive T cells developed spontaneous AIH-like disease (Figure 2), which could be classified in two distinct disease stages. Young Alb-iGP_Smartas mice (4-20 weeks; 'early stage') presented without apparent disease symptoms (Figure 2A), had normal serum transaminases (Figure 2B), but manifested portal infiltration in liver histology (Figure 2C, upper panels). Beginning at an age of 20 weeks ('late stage'), Alb-iGP_Smartas mice gradually manifested spontaneous sickness symptoms, such as reduced mobility, moderate piloerection, and altered facial expression or posture (Figure 2A). At 30 weeks of age, 50% of the mice manifested disease symptoms. This phenotypical sickness was always associated with significantly elevated serum transaminase levels (late stage ALT: $p=0.0312$; AST: $p=0.0006$; Figure 2B). The predominant histological picture of these apparently sick mice was that of portal lymphocytic infiltrates with interface hepatitis (Figure 2C; lower panels). Accordingly, histological activity, scored by a pathologist using the mHAI score, was significantly elevated already in the early stage in Alb-iGP_Smartas mice, as compared to Alb-iGP control mice ($p=0.0048$), and significantly increased further in Alb-iGP_Smartas mice in late stage ($p=0.0001$; Figure 2D). Moreover, Alb-iGP_Smartas mice had elevated serum IgG levels, both in early and late stage (Figure 2E; $p=0.0285$ and $p=0.0174$), and accumulated plasma cells in the liver (Figure 2F; $p=0.0159$ and $p=0.0286$). Accordingly, Alb-iGP_Smartas mice developed antinuclear autoantibodies (ANA) at relevant titres already in early stage (Figure 2G). The penetrance of typical AIH features in early and late stage is summarized in Table 1.

Pathogenic maturation of GP-reactive CD4 effector T cells within the livers of GP peptide-expressing mice

Histological analysis suggested that hepatic infiltrates in Alb-iGP_Smart mice, both in early and late disease stage, consisted mainly of CD4 T cells (Figure 3A, red); however some CD8 T cells (green) were also found, notably in the late stage. Since the development of AIH-like disease in Alb-iGP_Smart mice seemed to be driven by activation of autoreactive CD4 T cells, we analysed the liver-infiltrating T cells in the early stage. A significant increase of CD4 T cells numbers in livers of Alb-iGP_Smart mice was confirmed by flow cytometry as compared to Alb-iGP control mice that express GP in the liver but lack GP-specific T cells (Figure 3B). The majority of the liver infiltrating CD4 T cells recognized the I-A(b) LCMV GP66-77 tetramer (Figure 3C; the gating strategy and representative staining is shown in Supplementary Fig. 1), and displayed an activated effector or memory T cell phenotype (Figure 3D and Supplementary Figure 2A; $p=0.0005$), as compared to Smarta control mice that feature GP-specific T cells but lack GP expression in the liver. The liver infiltrating CD4 T cells in Alb-iGP_Smart mice were dominated by Th1 cells producing IFN γ (37.5%, Figure 3E; $p=0.0012$), which was a significant increase as compared to Alb-iGP control mice (8.6%). Interestingly and in accordance with our recent findings in human AIH (36), the liver infiltrating Th1 cells in Alb-iGP_Smart mice were marked by co-production of IFN γ and TNF in liver (Figure 3F and Supplementary Figure 2B; $p=0.0012$), indicating potent inflammatory activation. The fraction of IL-17 producers among the intrahepatic CD4 T cells was also elevated in Alb-iGP_Smart mice (14.8 vs. 2.2% in Alb-iGP controls; Figure 3G, $p=0.0003$). Corresponding to the predominant Th1 phenotype of the intrahepatic CD4 T cells, we found elevated expression of *Il12a* (Figure 3H, $p=0.0048$) and *Il12b* (Figure 3H, $p=0.0003$) in the livers of Alb-iGP_Smart mice. Accordingly, expression of the IL-12 receptor genes *Il12rb1* (Figure 3I, $p=0.0002$) and *Il12rb2* (Figure 3I, $p=0.0024$) were also upregulated in the livers of Alb-iGP_Smart mice.

To understand how the inflammatory activation of the autoreactive CD4 T cells occurred in the liver, we purified hepatocytes from Alb-iGP_Smart mice, or from Alb-iGP or Smarta

control mice and analysed the expression of the cognate GP peptide and of MHC II molecules in hepatocytes by quantitative RT-PCR. Both, expression of the GP peptide (Figure 4A, $p=0.0002$) and of the MHC II molecule I-A^b (Figure 4B, $p=0.0023$) were significantly up-regulated in 8 weeks old Alb-iGP_Smart mice. To confirm this finding, we performed immunofluorescence staining of liver sections for MHC II and for CD45, to unequivocally distinguish CD45- hepatocytes from CD45+ APCs. We found that some hepatocytes indeed did up-regulate MHC II molecules (Figure 4C); however, the majority of hepatocytes did not show detectable levels of MHC II. Thus, hepatocytes presenting GP peptides at low level seemed to participate in the inflammatory activation of autoreactive CD4 T cells in Alb-iGP_Smart mice, but probably not as major drivers. Yet we also found many CD45+ MHC II-expressing APCs in the livers of these mice, which prompted us to investigate these cells further. In flow cytometry, we observed a significant increase of CD11c+ DCs in the livers of Alb-iGP_Smart mice (Figure 4D; $p=0.0159$), whereas Ly6C^{hi} CD11b+ monocytes (Figure 4E; $p=0.1905$) or Ly6G+CD11b+ granulocytes (Figure 4F; $p=0.0159$) were not increased. To confirm that DCs might also drive tissue inflammation in human AIH, liver biopsies from 4 patients with active, newly diagnosed AIH before treatment were analysed histologically (Figure 4G, Table 2). Indeed, in contrast to pseudo-healthy control tissue from 2 subjects undergoing bariatric surgery, CD11c+ DCs were abundantly present in hepatic infiltrates in all studied AIH samples (Figure 4G).

The inflammatory activation of liver-infiltrating CD4 T cells seemed to occur mainly in the portal tracts of Alb-iGP_Smart mice, as suggested by the histological picture of considerable periportal infiltrates in the early disease stage (Figure 2C, Table 1). We noted that these early stage periportal infiltrates often had the appearance of ectopic lymphoid tissue. To confirm this unexpected finding, we performed additional immunohistochemical staining and found the characteristically segregated T and B cell zones in periportal infiltrates, which are typical for ectopic lymphoid tissue (Figure 5A,B). Moreover, we detected the typical network of dendritic cells (Figure 5C) and presence of high endothelial venules (Figure 5D), confirming the formation of ELTs in the livers of Alb-iGP_Smart mice at early

stage of AIH. Of note, these ELTs had been completely disaggregated in the late disease stage of Alb-iGP_Smart mice, in which the ELT had apparently merged into the more extensive, less ordered and dispersed infiltrates of interface hepatitis. These findings suggested that hepatic ELTs, which normally remain undetected in preclinical human AIH, might be a relevant site of inflammatory activation of autoreactive T cells.

Selective instability and reduced suppressor function in GP-reactive Tregs

The question then was why autoreactive effector T cell activation was not restricted by Tregs. To elucidate the possible role of Tregs in AIH pathogenesis, we first analysed thymic and peripheral Treg generation in Alb-iGP_Smart mice (Figure 6A), and found that thymic Treg induction was negligible, whereas peripheral Treg induction was significantly increased in Alb-iGP_Smart mice (6.1% splenic Tregs), as compared to Smart mice that do not feature the GP61-80 autoepitope (1.8% splenic Tregs; $p=0.068$) (Figure 6B). As indicated by immunohistochemical staining of Alb-iGP_Smart livers, Foxp3^+ Tregs were present in the early disease stage, but greatly reduced in the late disease stage (Figure 6C). This finding was confirmed by flow cytometry ($p=0.0079$; Figure 6D). These findings indicated that the expansion of Smart effector cells in late disease was associated with and probably enabled by greatly reduced Treg numbers.

To better understand how this Treg reduction could have occurred, we analysed the intrahepatic and splenic Foxp3^+ Tregs in the early disease stage. Intriguingly, we found that the expression of Foxp3 was selectively reduced in the GP-specific Tregs, (Figure 7A and supplementary Figure 3A), as indicated by significantly decreased mean fluorescence intensity (MFI) of Foxp3 in comparison to the Foxp3 MFI of non-specific Tregs (liver: 686.8 vs. 1086, $p<0.0001$; spleen: 568 vs. 835; $p=0.0286$). Note that stable maintenance of Foxp3 expression is important for Treg function, and reduced Foxp3 expression can indicate Treg instability and reduced Treg function (33, 37, 38). Stable Foxp3 expression is mainly maintained by epigenetic modification of the Foxp3 gene locus and, in particular, by full demethylation of the conserved non-coding DNA sequence element 2 (CNS2) (also known

as the Treg-specific demethylated region) (38, 39, 40). Thus, to confirm that GP-specific Tregs exhibited reduced stability, we sorted pooled antigen-specific or non-specific splenic Tregs of 10 mice, based on tetramer-binding and *Foxp3*-gfp reporter activity, taking advantage of *Foxp3*-gfp reporter mice (41) bred onto Alb-iGP_Smarta background. Demethylation analysis of the CNS2 element revealed that the GP-specific Tregs showed a considerably reduced degree of *Foxp3* gene demethylation, as compared to non-specific Tregs (88% vs. 100%; Figure 7B). As a consequence of the selective instability of antigen-specific Tregs, their frequency declined significantly between week 8 of age, when about 75% of all Tregs were antigen-specific, and week 20, when only about 30% antigen-specific Tregs remained (Figure 7C; $p < 0.0001$). Note that, in contrast, the overall Treg frequency did not change significantly between weeks 8 and 20 (Figure 7D).

We tested whether the instability of GP-specific Tregs was associated with reduced expression of the functional molecule CD39 (Figure 7E). We found indeed that CD39 was reduced in splenic ($p=0.0079$), as well as intrahepatic GP-specific Tregs ($p=0.0079$), as compared to non-specific Tregs. Moreover, a significantly increased proportion of the splenic as well as intrahepatic GP-specific Tregs produced IL-17 (Figure 7F and supplementary Figure 3B), as compared to non-specific intrahepatic Tregs (liver: 33.4% vs. 16.3%; $p=0.0286$; spleen: 16.8 vs. 8.4; $p=0.0286$). Note that such Th17-like phenotype in Tregs indicates a reversible loss of suppressor activity (42). Moreover, again using *Foxp3*-gfp reporter activity to sort GP-specific or non-specific Tregs, we could directly compare their suppressive capacity in an *in vitro* suppression assay. As can be seen in Figure 7G, GP-specific Tregs were significantly less functional as suppressors as non-specific Tregs ($p < 0.0001$). These findings demonstrated that the GP-specific Tregs were indeed selectively impaired in Alb-iGP_Smarta mice.

Discussion

The mechanisms that allow autoreactive T cells to defy immune regulation and to cause self-sustained autoimmune diseases are not fully understood. In particular, it is unclear how the loss of tolerance to tissue-restricted antigens might occur at immune-privileged sites like the liver. Here, we describe a new mouse model of spontaneous CD4 T cell-driven AIH, which allowed us to address several key questions related to the break of tolerance in the liver and the pathogenesis of AIH.

1) What is the role of thymic tolerance in autoimmune pathogenesis?

In the thymus, the medullary thymic epithelial cells can induce tolerance to many self-antigens, including liver antigens. They can do this because these cells feature several transcriptional programmes coordinated by the transcription factors Aire, Fezf2 and Prdm1, which facilitate the ectopic expression of a wide array of tissue-restricted antigens (43-45). However, different self-antigens vary in their degree of thymic representation, and these representation patterns have been demonstrated to determine the fate of the immature T cells in the thymus. Indeed, Malhotra et al showed that 1) peptides that are uniformly presented by thymic antigen-presenting cells produce clonal deletion, 2) peptides with limited thymic expression induce partial clonal deletion and thymic generation of Tregs, and 3) peptides that are excluded from thymus are ignored (46). Thus, autoreactive T cells recognizing tissue-restricted autoantigens, which are rarely expressed in the thymus, are prone to escape clonal deletion. Our model confirmed that assumption by showing that GP-specific CD4 T cells were not deleted in the thymus of Alb-iGP_Smart mice, due to absent thymic GP expression (Figure 1); in contrast, the high degree of thymic GP expression in Itgax-iGP_Smart mice was associated with near complete deletion of autoreactive CD4 T cells. Importantly, as a consequence of the absent deletion in the thymus of Alb-iGP_Smart mice, autoreactive T cells abounded in the periphery. Upon antigen recognition in the liver, the autoreactive effector cells were activated, enabling spontaneous development of the typical disease features of autoimmune hepatitis (Table1, Figure 2).

2) What drives the activation of autoreactive effector T cells?

We found that the pathogenic activation of the previously ignorant GP-reactive CD4 T cells in Alb-iGP_Smart mice seemed to require several weeks of subclinical autoimmunity before the spontaneous clinical manifestation of self-sustained autoimmune disease. Of note, this pathogenic maturation seemed to occur in the liver. Indeed, we found that at least some hepatocytes had up-regulated MHC II expression (Figure 4B,C), which hence might have contributed to the activation of GP-reactive CD4 T cells. However, we also observed a substantial expansion of DCs in the livers already in young Alb-iGP_Smart mice (Figure 4D), indicating that DCs, being potent professional APCs, most likely were the major drivers of the pathogenic activation of previously ignorant autoreactive CD4 effector T cells. Importantly, we also find a substantial expansion of CD11c+ DCs in human treatment-naïve AIH (Figure 4G). In mice, we often observed the transient formation of portal ectopic lymphoid tissue in Alb-iGP_Smart mice (Figure 5). Ectopic lymphoid tissues are organized structures of T cells together with antigen-presenting cells that are suspected to boost autoimmune pathogenesis (20). For yet unclear reasons, these highly ordered ectopic lymphoid structures seemed to disaggregate in later disease. Whether similar, transient structures might also be involved in preclinical stages of human AIH is currently not clear, as human AIH is usually diagnosed only in the clinical disease stage in which these structures were also absent in mice. Yet, irrespective of the microanatomical specifics, our model revealed that intrahepatic expansion of professional APCs seems to be a characteristic of both human and murine AIH, providing a stimulation platform for the inflammatory activation of autoreactive T cells locally in the liver. This pathogenic activation seemed to involve IL-12 (Figure 3H,I), which is the major driver of Th1-like effector T cell responses. Accordingly, the pathogenic activation of GP-reactive CD4 T cells in mice was marked by co-production of the classical Th1 cytokines IFN γ and TNF (Figure 3F). Of note, we find a similar dominance of IFN γ and TNF co-producers among the liver-infiltrating CD4 T cells in human AIH (36), indicating that this cytokine signature might be relevant for AIH pathogenesis. Our findings

re-emphasise the previously reported pathogenic role of IL-12 in murine AIH (19). Therefore, intrahepatically expanded DCs and the DC-derived cytokine IL-12 might be relevant treatment targets in AIH that should be explored in future studies.

3) *What is the role of regulatory T cells in the break of tolerance to liver antigens?*

Tregs have the potential to suppress the activation of autoreactive effector T cells that have escaped clonal deletion, most notably when they recognize the same autoantigen as the effectors (6, 24). Importantly, GP-reactive Tregs were present in early stage AIH livers of Alb-iGP_Smart mice (Figure 6). This is reminiscent of human AIH in which several groups have reported that Tregs do accumulate in inflamed AIH livers (27, 28, 29). Yet, both the human and murine intrahepatic Tregs do not seem to be effective in suppressing effector T cells in the inflamed liver. Here, we show that this functional deficit might be explained by Treg instability and plasticity, which selectively occurred in autoantigen-specific, but not in non-specific Tregs. Importantly, this instability produced a significant reduction of the antigen-specific Tregs during the preclinical stage between week 8 and week 20 of age, whereas non-specific Tregs remained stable (Figure 7C,D). Treg instability and plasticity was marked by reduced *Foxp3* expression, reduced demethylation of the CNS2 element at the *Foxp3* gene locus, reduced expression of the functional marker CD39, and production of IL-17 (Figure 7 E,F). Of note, these antigen-specific Tregs exhibited reduced suppressive activity, as compared to non-specific Tregs (Figure 7G). The precise mechanisms leading to Treg instability and plasticity are not clear; however, these phenomena have been linked to autoimmune disorders (32, 33). Under the influence of inflammatory cytokines, Tregs can convert into Th-like cells that also produce effector cytokines while maintaining *Foxp3* expression (33, 47, 48, 49). Here we find that Tregs acquired Th17-like features, an adaptation that has been reported to result in reduced suppressive potential under inflammatory conditions (42, 47). Thus far, it is not clear whether Th17-like Tregs are a stable cell type or represent an intermediate state in a conversion process (50, 51). Nonetheless, our finding is important, as it demonstrates that AIH pathogenesis does not require a

generalized Treg defect, as had been proposed before (26). In contrast, Treg dysfunction in AIH seems to occur selectively in autoantigen-specific Tregs. These antigen-specific Tregs might have been prone to become instable due to their peripheral, not thymic origin (see Figure 6), as peripherally induced Tregs usually feature lower CNS2 demethylation and reduced stability as compared to thymus-induced Tregs (38, 39). Moreover, we think that antigen-specific Treg instability was most likely an adaptation to inflammatory conditions in the liver (52). Note that we have previously identified IL-12 as an important mediator of intrahepatic Treg dysfunction under inflammatory conditions (31). We find it thus most likely that the here identified hepatic up-regulation of IL-12 not only had driven the pathogenic effector cell activation, as explained above, but also the observed instability of the antigen-specific Tregs.

Due to its similarities to human AIH, we think that this new AIH model provides a valuable paradigm to uncover immune mechanisms of the thus far elusive pathogenesis of AIH and to identify potential treatment targets. Yet it seems to be less suited for treatment studies, given its variable disease onset and rapid progression. Moreover, the model does not show the sexual dimorphism in disease prevalence that is found in human disease. However, as an explanation for female preponderance of autoimmunity, it has been suggested that female sex hormones repress AIRE expression in the thymus, allowing more autoreactive T cells to escape thymic selection (53). It is thus conceivable that our model did not manifest a sexual dimorphism, because thymic GP expression was virtually absent in both sexes and thus not influenced by sex hormones.

In summary, our model revealed that AIH seems to be driven by activation of previously ignorant autoreactive CD4 effector T cells and differentiation towards IFN γ and TNF co-producers. Effector cell activation and differentiation seemed to be induced locally in the liver by an expanded population of intrahepatic DCs. Moreover, the autoantigen-specific Tregs in the inflamed liver, but not the non-specific Tregs, selectively manifested increased plasticity

and instability, suggesting that Treg dysfunction in AIH is not generalized, but restricted to autoreactive Tregs. Thus, autoimmune pathogenesis in an immune-privileged organ like the liver seems to require both, insufficient thymic deletion of autoreactive T cells and maladaptive peripheral regulation caused by instability of autoantigen-specific Tregs. Therefore, the success of Treg-based treatment attempts for autoimmune diseases affecting immune-privileged organs might depend on additional strategies to stabilize antigen-specific Treg phenotype and function.

Methods

Generation of invariant chain GP (iGP) mice

The targeting vector ROSA26STOP*liMOG (34), a gift from A. Waisman (University Medicine Mainz, Germany), was used to generate the targeting vector ROSA26STOP*iGP by replacement of the MOG peptide encoding gene sequence with a gene sequence encoding the immunodominant GP peptide of lymphocytic choriomeningitis virus (LCMV). To that end, we generated the mutant invariant chain (iGP) by assembly PCR on the liMOG template cDNA (34), replacing the coding sequence of the MOG peptide with that of GP61-80 peptide in the correct reading-frame. This was done by amplifying two fragments of either the 5' or the 3' part of the invariant chain sequence using one of the two external primers li-fwd (5'-GGATCTGACATGGTAAGTAA-3') and li-rev (5'-CGTATAGCATACATTATACG-3'), in conjunction with one of two internal primers that were used to replace the MOG sequence by the GP sequence: (GP-fwd: 5'-CCCCGACATCTA CAAGGGCGTGTACCAGTTCAAGTCCGTGGAGTTCGACGATAACATGCTCCTGGGCC-3', and GP-rev: 5'-CGGACTTGAACCTGGTACACGCCCTGTAGATGTCGGGGCCGTTCAAGGCCCTTCATGCG AAGGCTCTCCA-3'). The two fragments were assembled by PCR using the external primers li-fwd and li-rev to obtain one iGP minigene (886 bp) introducing one Ascl restriction site to the 5' end and one Fsel restriction site to the 3' end. The obtained iGP minigene was amplified after cloning into the pGEM-T Easy vector (Promega). The original targeting vector ROSA26STOP*liMOG, as well as the iGP minigene were restricted with Ascl and Fsel, followed by ligation of the two resulting gene fragments of 750 bp and 14.2 kb. The targeting vector was linearized with Pvul and electroporated into ES cells, which were cultivated as described (54). Homologous recombinants were identified by Southern blot analysis using a 700bp genomic EcoRI-Pacl fragment after EcoRI digest (data not shown). Chimeras were generated from two homologous recombinant clones by injection into blastocysts. Germline transmission was confirmed by Southern blot analysis after EcoRI digest using a 1-kb SacII-

XbaI fragment (probe 1; p1) from pROSA26-1. ES cell culture, targeting and implantation was performed by Irm Hermans-Borgmeyer (Center for Molecular Neurobiology Hamburg).

Animal experimentation

To achieve conditional expression of the GP peptide in hepatocytes, iGP mice were crossed with Smarta mice (35), and the resulting iGP_Smart mice were then further bred with Alb-Cre mice to create Alb-iGP_Smart mice that feature both, hepatocellular expression of the GP61-80 peptide and CD4 T cells recognizing the GP61-80 peptide sequence. Accordingly, to obtain Itgax-iGP_Smart mice with GP61-80 expression mainly restricted to dendritic cells, iGP_Smart mice were bred with Itgax-Cre mice. As indicated, Foxp3gfp.KI reporter mice (41) were backcrossed onto the Alb-iGP_Smart background. All mice were bred and kept under specific pathogen-free conditions with 12 hours light/dark cycles in the animal facility of the University Medical Center Hamburg-Eppendorf with access to water and standard chow diet (1318 rodent diet, Altromin) ad libitum. The mice were monitored daily for sickness symptoms, according to general appearance, body condition, posture, facial expression and mobility, for a period of up to 60 weeks. Clinical and behavioural humane endpoints were applied to minimize any harm. All animals received humane care and all animal experiments were carried out in accordance with the principles of the Basel Declaration and the European Directive 2010/63/EU.

Cell isolation

Primary cells were isolated from thymus, spleen, or liver. In brief, organs were passed through a 100µM cell-strainer to obtain single cell suspensions. For isolation of liver non-parenchymal cells, the liver cell suspension was further purified by density gradient centrifugation as described (55). Regulatory T cells were isolated from spleens of Foxp3gfp.KI reporter mice crossed onto Alb-iGP_Smart background by fluorescence-based flow cytometrical sorting with a BD Aria III (BD Biosciences). These cells were then either subjected to DNA extraction with the DNeasy blood and tissue kit (Qiagen), followed by

determination of the Foxp3 gene locus demethylation at Epiontis GmbH, Berlin, or used in functional suppression assays described below. Hepatocytes were isolated as described (56).

Flow cytometry

Single cell suspensions were stained with PacificOrange™ (Life Technologies) for dead cell exclusion, and further stained for CD45 (clone 30-F11), CD4 (RM4-5), CD62L (MEL-14), CD39 (Duha59), CD19 (1D3), CD138 (281-2), TNF (MP6-XT22), IL-17 (TC11-18H10.1) (BioLegend), CD8 (53-6.7), CD44 (IM7), IFN γ (XMG1.2), (BD Bioscience) or Foxp3 (FJK-16S) (ThermoFisher Scientific) using fluorochrome-labelled antibodies. As indicated, cells were also stained with APC-conjugated I-A(b) LCMV GP 66-77 tetramer, which was obtained from the NIH Tetramer Core Facility. The FoxP3 staining buffer set (ThermoFisher Scientific) was used for Foxp3 and intracellular cytokine staining following re-stimulation *in vitro* with PMA/Ionomycin (Sigma-Aldrich) for 5 hours in the presence of the Golgi inhibitor GolgiPlug (BD Biosciences).

Suppression assay

In vitro suppression assays were performed as described (57). Briefly, purified antigen-specific and non-specific Foxp3+ Tregs were sorted from Foxp3gfp.KI reporter mice on Alb-iGP_Smarta background based on binding of APC-conjugated I-A(b) LCMV GP 66-77 tetramer and gfp reporter signals. Tregs were co-cultured with splenic CD4+CD25- non-Tregs from C57BL/6 mice stained with CellTraceTM Violet Cell Proliferation Kit (Life technologies) according to the manufacturer's instructions prior to the cell culture. After stimulation in the presence of 1 μ g/ml anti-CD3 (145-2C11) and 1 μ g/ml anti-CD28 (37.51) antibodies (BioLegend) for three days in IMDM/10%FCS (Gibco), T cell proliferation was assessed by flow cytometry.

Gene expression analysis

For quantitative gene expression analysis, RNA was extracted from liver or thymus tissue with the NucleoSpin® RNA kit (Macherey-Nagel) and reverse-transcribed with the High capacity cDNA Reverse Transcriptase Kit (ThermoFisher Scientific) according to the manufacturer's protocol. The cDNA was then subjected to real-time quantitative PCR using the Powerup SYBR green master mix (ThermoFisher Scientific). GP target gene expression was detected using the primers CD74-fw (5'-CACTACTGCTTACTCCTGT-3') and GP-rev (5'-TCCACGGACTTGAACCTGGTA-3') (Eurofins), and normalized to mHprt house keeper levels using the primers mHprt-fw: 5'-GTTGGATACAGGCCAGACTTGTTG-3' and mHprt-rev: 5'-CTAATTTACTGGCAACATCAACAG-3' (Eurofins) by employing the $\Delta\Delta Ct$ method. Alternatively, TaqMan™ Gene Expression Assays (ThermoFisher Scientific) were used: *H2-Ab1*, Mm00439216_m1; *Il12a*, Mm00434169_m1; *Il12b*, Mm01288989_m1; *IL12rb1*, Mm00434189_m1; *Il12rb2*, Mm00434200_m1.

Immunohistology and fluorescence microscopy

For analysis of liver inflammation, sections from *in situ* perfused and paraffin-fixed mouse livers were stained with hematoxylin and eosin (Roth) and scored by our pathologist in a blinded fashion applying the mHAI score (58). To visualize CD4+ T cells, Foxp3+ Tregs, B220+ B cells, CD11c+ DCs (human and mouse) or PNAd+ high endothelial venules, the POLAP-Kit: Zytocell-Plus AP-Polymer-Kit (Zytomed Systems) and the respective antibodies (PNAd antibody from BioLegend (MECA-79), CD11c from Invitrogen (PAS-79537), all other from ThermoFisher Scientific (4SM95, FJK-16S, RA3-6B2, M5/114.15.2) were used. Aceton-fixed cryosections of snap-frozen livers were stained with directly fluorochrome-labelled antibodies to CD4 (GK1.5), CD8 (53-6.7) and CD45 (104) (BioLegend), or with rat anti-mouse MHCII (Invitrogen) followed by incubation with goat anti-rat IgG AF546 (Invitrogen A11081) and counterstained with the nuclear dye Hoechst 33258.

Antinuclear antibody (ANA) detection

ANA were detected by indirect immunofluorescence using BIOCHIP slides (EUROIMMUN) loaded with human Hep2 cells, which were incubated with serial dilutions of mouse sera. Specific serum autoantibody binding was then visualized by immunofluorescence microscopy.

Serology

To assess liver damage, serum alanine aminotransferase (ALT) and aspartate aminotransferase (AST) levels were measured at the Institute of Experimental Immunology and Hepatology, University Medical Centre Hamburg-Eppendorf, using a COBAS Mira System (Roche Diagnostic). IgG serum titres were measured with the IgG mouse ELISA Kit (Abcam). Serum cytokines were analysed with the Milliplex MAP mouse cytokine/chemokine kit (Merckmillipore) according to the manufacturer's instructions.

Statistics

For statistical analysis of two groups, the Mann-Whitney test was applied. For comparison of more groups, the one-way ANOVA test followed by Tukey's post test was performed. Significance of ANA data was calculated with Fisher's exact test with a cut-off titre of 1:80. Disease incidence was analysed using the log-rank (Mantel-Cox) test. $P<0.05$ was considered as significant. Results in graphs are displayed as mean \pm SEM.

Study approval

Animal studies have been approved by the review board of the State of Hamburg, Germany. The use of human liver specimens for histological analysis was approved by the responsible ethics committee of the 'Landesärztekammer Hamburg' (reference number PV3912).

Author contributions

Study concept and design: M Preti, A Carambia, J Herkel

Experimental work and data analysis: M Preti, L Schlott, D Lübbingering, D Krzikalla, AL Müller, M Schakat, S Weidemann, A Carambia

Drafting of the manuscript: M Preti, A Carambia, J Herkel

Technical or material support: AW Lohse, C Weiler-Normann, D Schwinge, C Schramm, M Sebode

Funding acquisition: J Herkel

All authors critically revised and approved the manuscript, and accepted accountability.

Acknowledgements

This study was supported by the DFG - Deutsche Forschungsgemeinschaft (SFB841 and KFO306). We thank the National Institutes of Health Tetramer Core Facility for generous provision of APC-conjugated I-A(b) LCMV GP 66-77 tetramer. We thank Marko Hilken, Sabrina Kress, Carsten Rothkegel, Angelika Schmidt, Nina Verse and Jenny Wigger for excellent technical assistance. We are grateful to Ari Waisman, University Medicine Mainz, Germany for kindly providing the ROSA26STOP*liMOG targeting vector, to Irm Hermans-Borgmeyer, Center for Molecular Neurobiology Hamburg, for excellent ES cell targeting and implantation service, and to Thomas Korn for kindly providing Foxp3gfp.KI reporter mice. Cell sorting was performed in the flow cytometry core facility of the University Medical Centre Hamburg-Eppendorf. Human samples were kindly provided by the Liver.net biobank of the SFB841.

References

1. Davidson A, Diamond B. Autoimmune diseases. *N Engl J Med.* 2001;345:340-350.
2. Ben-Nun A, Wekerle H, Cohen IR. The rapid isolation of clonable antigen-specific T lymphocyte lines capable of mediating autoimmune encephalomyelitis. *Eur J Immunol.* 1981;11:195-199.
3. Hogquist KA, Jameson SC. The self-obsession of T cells: how TCR signaling thresholds affect fate 'decisions' and effector function. *Nat Immunol.* 2014;15:815-23.
4. Theofilopoulos AN, Kono DH, Baccala R. The multiple pathways to autoimmunity. *Nat Immunol.* 2017;18:716-724.
5. Legoux FP, et al. CD4+ T Cell Tolerance to Tissue-Restricted Self Antigens Is Mediated by Antigen-Specific Regulatory T Cells Rather Than Deletion. *Immunity.* 2015;43:896-908.
6. Sakaguchi S, Yamaguchi T, Nomura T, Ono M. Regulatory T cells and immune tolerance. *Cell.* 2008;133:775-787.
7. Carambia A, Herkel J. Dietary and metabolic modulators of hepatic immunity. *Semin Immunopathol.* 2018;40:175-188.
8. Thomson AW, Knolle PA. Antigen-presenting cell function in the tolerogenic liver environment. *Nat Rev Immunol.* 2010;10:753-766.
9. Calne RY, et al. Induction of immunological tolerance by porcine liver allografts. *Nature.* 1969;223:472-476.
10. Lüth S, et al. Ectopic expression of neural autoantigen in mouse liver suppresses experimental autoimmune neuroinflammation by inducing antigen-specific Tregs. *J Clin Invest.* 2008;118:3403-3410.
11. Carambia A, et al. Nanoparticle-based autoantigen delivery to Treg-inducing liver sinusoidal endothelial cells enables control of autoimmunity in mice. *J Hepatol.* 2015;62:1349-56.
12. Manns MP, Lohse AW, Vergani D. Autoimmune hepatitis--Update 2015. *J Hepatol* .2015;62:S100-111.

13. Hardtke-Wolenski M, Taubert R, Jaeckel E. Animal models for autoimmune liver disease--what is relevant for immune-mediated liver disease. *Dig Dis.* 2012;30:2-10.
14. Hardtke-Wolenski M, et al. Genetic predisposition and environmental danger signals initiate chronic autoimmune hepatitis driven by CD4+ T cells. *Hepatology.* 2013;58:718-728.
15. Lapierre P, Djilali-Saiah I, Vitozzi S, Alvarez F. A murine model of type 2 autoimmune hepatitis: Xenoimmunization with human antigens. *Hepatology.* 2004;39:1066-1074.
16. Holdener M, et al. Breaking tolerance to the natural human liver autoantigen cytochrome P450 2D6 by virus infection. *J Exp Med.* 2008;205:1409-1422.
17. Zierden M, Kühnen E, Odenthal M, Dienes HP. Effects and regulation of autoreactive CD8+ T cells in a transgenic mouse model of autoimmune hepatitis. *Gastroenterology.* 2010;139:975-986.
18. Bonito AJ, et al. Medullary thymic epithelial cell depletion leads to autoimmune hepatitis. *J Clin Invest.* 2013;123:3510-3524.
19. Gil-Farina I, et al. Transient Expression of Transgenic IL-12 in Mouse Liver Triggers Unremitting Inflammation Mimicking Human Autoimmune Hepatitis. *J Immunol.* 2016;197:2145-2156.
20. Corsiero E, Nerviani A, Bombardieri M, Pitzalis C. Ectopic Lymphoid Structures: Powerhouse of Autoimmunity. *Front Immunol.* 2016;7:430.
21. Jones GW, Jones SA. Ectopic lymphoid follicles: inducible centres for generating antigen-specific immune responses within tissues. *Immunology.* 2016;147:141-151.
22. Grant AJ, et al. Hepatic expression of secondary lymphoid chemokine (CCL21) promotes the development of portal-associated lymphoid tissue in chronic inflammatory liver disease. *Am J Pathol.* 2002;160:1445-1455.
23. Pikarsky E, Heikenwalder M. Focal and Local: Ectopic Lymphoid Structures and Aggregates of Myeloid and Other Immune Cells in Liver. *Gastroenterology.* 2016;151:780-783.

24. Herkel J. Regulatory T Cells in Hepatic Immune Tolerance and Autoimmune Liver Diseases. *Dig Dis.* 2015;33 Suppl 2:70-74.
25. Jeffery HC, Braitch MK, Brown S, Oo YH. Clinical Potential of Regulatory T Cell Therapy in Liver Diseases: An Overview and Current Perspectives. *Front Immunol.* 2016;7:334.
26. Ferri S, et al. A multifaceted imbalance of T cells with regulatory function characterizes type 1 autoimmune hepatitis. *Hepatology.* 2010;52:999-1007.
27. Peiseler M, et al. FOXP3+ regulatory T cells in autoimmune hepatitis are fully functional and not reduced in frequency. *J Hepatol.* 2012;57:125-132.
28. Taubert R, et al. Intrahepatic regulatory T cells in autoimmune hepatitis are associated with treatment response and depleted with current therapies. *J Hepatol.* 2014;61:1106-1114.
29. Oo YH, et al. Distinct roles for CCR4 and CXCR3 in the recruitment and positioning of regulatory T cells in the inflamed human liver. *J Immunol.* 2010;184:2886-2898.
30. Chen YY, et al. Human intrahepatic regulatory T cells are functional, require IL-2 from effector cells for survival, and are susceptible to Fas ligand-mediated apoptosis. *Hepatology.* 2016;64:138-150.
31. Schwinge D, et al. Dysfunction of hepatic regulatory T cells in experimental sclerosing cholangitis is related to IL-12 signaling. *J Hepatol.* 2017;66:798-805.
32. Kleinewietfeld M, Hafler DA. The plasticity of human Treg and Th17 cells and its role in autoimmunity. *Semin Immunol.* 2013;25:305-312.
33. Qiu R, et al. Regulatory T Cell Plasticity and Stability and Autoimmune Diseases. *Clin Rev Allergy Immunol.* 2020;58:52-70.
34. Frommer F, et al. Tolerance without clonal expansion: self-antigen-expressing B cells program self-reactive T cells for future deletion. *J Immunol.* 2008;181:5748-5759.
35. Oxenius A, Bachmann MF, Zinkernagel RM, Hengartner H. Virus-specific MHC-class II-restricted TCR-transgenic mice: effects on humoral and cellular immune responses after viral infection. *Eur J Immunol.* 1998;28:390-400.

36. Bovensiepen CS, et al. TNF-Producing Th1 Cells Are Selectively Expanded in Liver Infiltrates of Patients with Autoimmune Hepatitis. *J Immunol*. 2019;203:3148-3156.
37. Sakaguchi S, Vignali DA, Rudensky AY, Niec RE, Waldmann H. The plasticity and stability of regulatory T cells. *Nat Rev Immunol*. 2013;13:461-467.
38. Lu L, Barbi J, Pan F. The regulation of immune tolerance by FOXP3. *Nat Rev Immunol*. 2017;17:703-717.
39. Zheng Y, Josefowicz S, Chaudhry A, Peng XP, Forbush K, Rudensky AY. Role of conserved non-coding DNA elements in the Foxp3 gene in regulatory T-cell fate. *Nature*. 2010;463:808-812.
40. Ohkura N, et al. T cell receptor stimulation-induced epigenetic changes and Foxp3 expression are independent and complementary events required for Treg cell development. *Immunity*. 2012;37:785-99.
41. Korn T, et al. Myelin-specific regulatory T cells accumulate in the CNS but fail to control autoimmune inflammation. *Nat Med*. 2007;13:423-431.
42. Beriou G, et al. IL-17-producing human peripheral regulatory T cells retain suppressive function. *Blood*. 2009;113:4240-4249.
43. Peterson P, Org T, Rebane A. Transcriptional regulation by AIRE: molecular mechanisms of central tolerance. *Nat Rev Immunol*. 2008;8:948-57.
44. Takaba H, et al. Fezf2 Orchestrates a Thymic Program of Self-Antigen Expression for Immune Tolerance. *Cell*. 2015;163:975-87.
45. Roberts NA, et al. Prdm1 Regulates Thymic Epithelial Function To Prevent Autoimmunity. *J Immunol*. 2017;199:1250-1260.
46. Malhotra D, et al. Tolerance is established in polyclonal CD4(+) T cells by distinct mechanisms, according to self-peptide expression patterns. *Nat Immunol*. 2016;17:187-195.
47. Komatsu N, et al. Pathogenic conversion of Foxp3+ T cells into TH17 cells in autoimmune arthritis. *Nat Med*. 2014;20:62-8.

48. Massoud AH, Charbonnier LM, Lopez D, Pellegrini M, Phipatanakul W, Chatila TA. An asthma-associated IL4R variant exacerbates airway inflammation by promoting conversion of regulatory T cells to TH17-like cells. *Nat Med.* 2016;22:1013-22.
49. Hwang SM, Sharma G, Verma R, Byun S, Rudra D, Im SH. Inflammation-induced Id2 promotes plasticity in regulatory T cells. *Nat Commun.* 2018;9:4736.
50. Du R, Zhao H, Yan F, Li H. IL-17⁺Foxp3⁺ T cells: an intermediate differentiation stage between Th17 cells and regulatory T cells. *J Leukoc Biol.* 2014;96:39-48.
51. Afzali B, Mitchell P, Lechner RI, John S, Lombardi G. Translational mini-review series on Th17 cells: induction of interleukin-17 production by regulatory T cells. *Clin Exp Immunol.* 2010;159:120-130.
52. Korn T, Muschawec A. Stability and Maintenance of Foxp3⁺ Treg Cells in Non-lymphoid Microenvironments. *Front Immunol.* 2019;10:2634.
53. Berrih-Aknin S, Panse RL, Dragin N. AIRE: a missing link to explain female susceptibility to autoimmune diseases. *Ann N Y Acad Sci.* 2018;1412:21-32.
54. Köntgen F, Süss G, Stewart C, Steinmetz M, Bluethmann H. Targeted disruption of the MHC class II Aa gene in C57BL/6 mice. *Int Immunol.* 1993;5:957-964.
55. Schwinge D, et al. Testosterone suppresses hepatic inflammation by the downregulation of IL-17, CXCL-9, and CXCL-10 in a mouse model of experimental acute cholangitis. *J Immunol.* 2015;194:2522-2530.
56. Lüth S, et al. Chronic inflammatory IFN- γ signaling suppresses hepatocarcinogenesis in mice by sensitizing hepatocytes for apoptosis. *Cancer Res.* 2011;71:3763-71.
57. Carambia A, et al. TGF- β -dependent induction of CD4+CD25+Foxp3⁺ Tregs by liver sinusoidal endothelial cells. *J Hepatol.* 2014;61:594-9.
58. Ishak K, et al. Histological grading and staging of chronic hepatitis. *J Hepatol.* 1995;22:696-699.

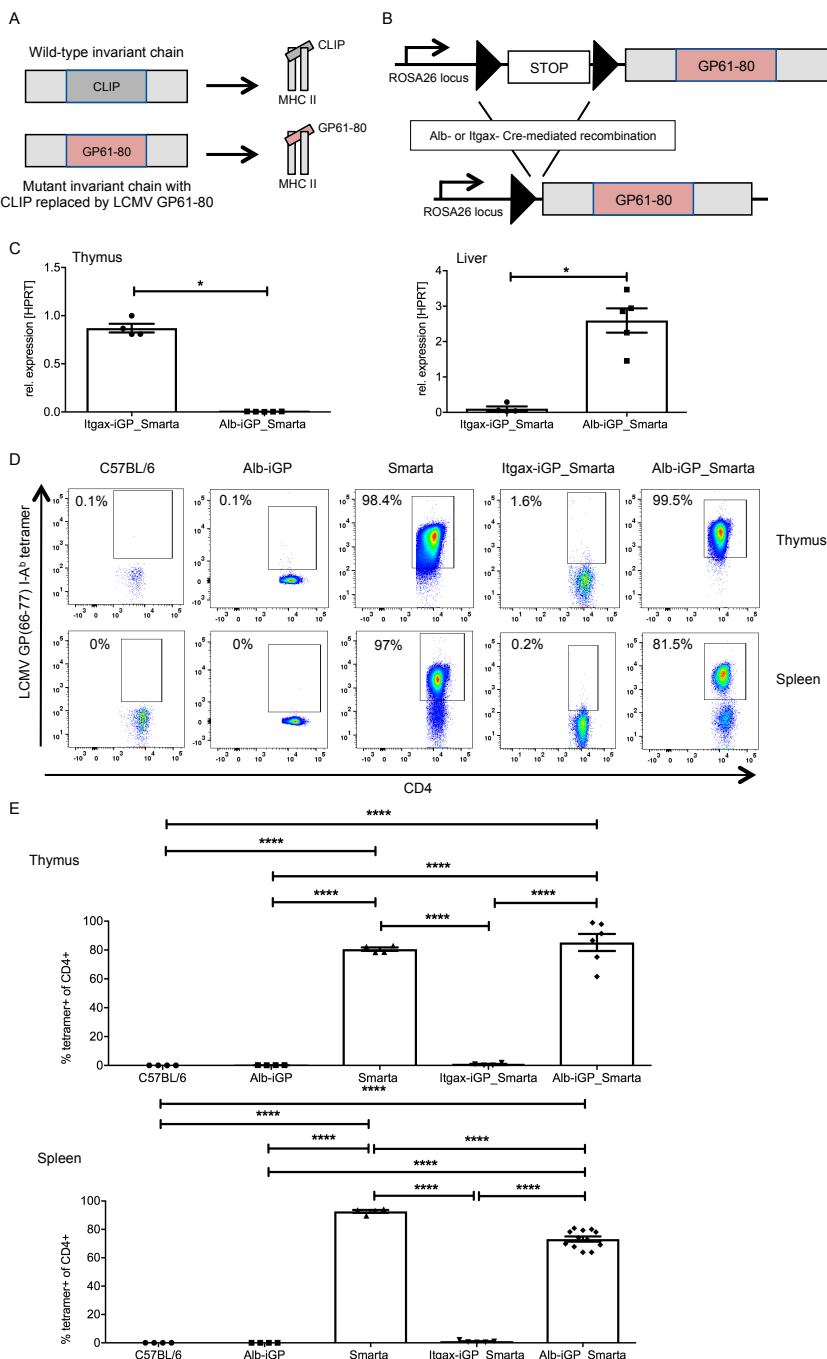


Figure 1: Generation of Alb-iGP_Smarta mice and characterization of thymic and peripheral autoreactive CD4 T cells. (A) Scheme of the Alb-iGP system. The CLIP sequence in the CD74 gene was replaced by the GP61-80 sequence, facilitating high occupancy of MHC II molecules and GP61-80 presentation. (B) Cre-mediated removal of a STOP cassette facilitates expression of the mutant CD74 molecule under Rosa26 promoter control. (C) GP61-80 expression levels in thymus and spleen of Itgax-iGP_Smarta and Alb-iGP_Smarta mice, as determined by quantitative RT-PCR relative to the HPRT housekeeper

gene expression. (D) Representative flow cytometry dot plots of antigen-specific I-A(b) GP66-77 tetramer-binding CD4 T cells in thymus (upper panels) or spleen (lower panels) in C57BL/6 mice, Alb-iGP mice expressing the mutant CD74 molecule, Smarta mice expressing a transgenic T cell receptor recognizing the cognate GP61-80 peptide, Itgax-iGP_Smartas mice or Alb-iGP_Smartas mice, featuring both, presentation of the GP61-80 peptide and the cognate Smarta T cell receptor. (E) Thymic (left) and splenic (right) frequencies of I-A(b) GP66-77 tetramer-specific CD4 T cells in C57BL/6, Alb-iGP, Smarta, Itgax-iGP_Smartas, or Alb-iGP_Smartas mice. Shown are mean and SEM ($n = 4-12$). * $p < 0.05$; *** $p < 0.0001$ (C: Mann-Whitney; E: ANOVA).

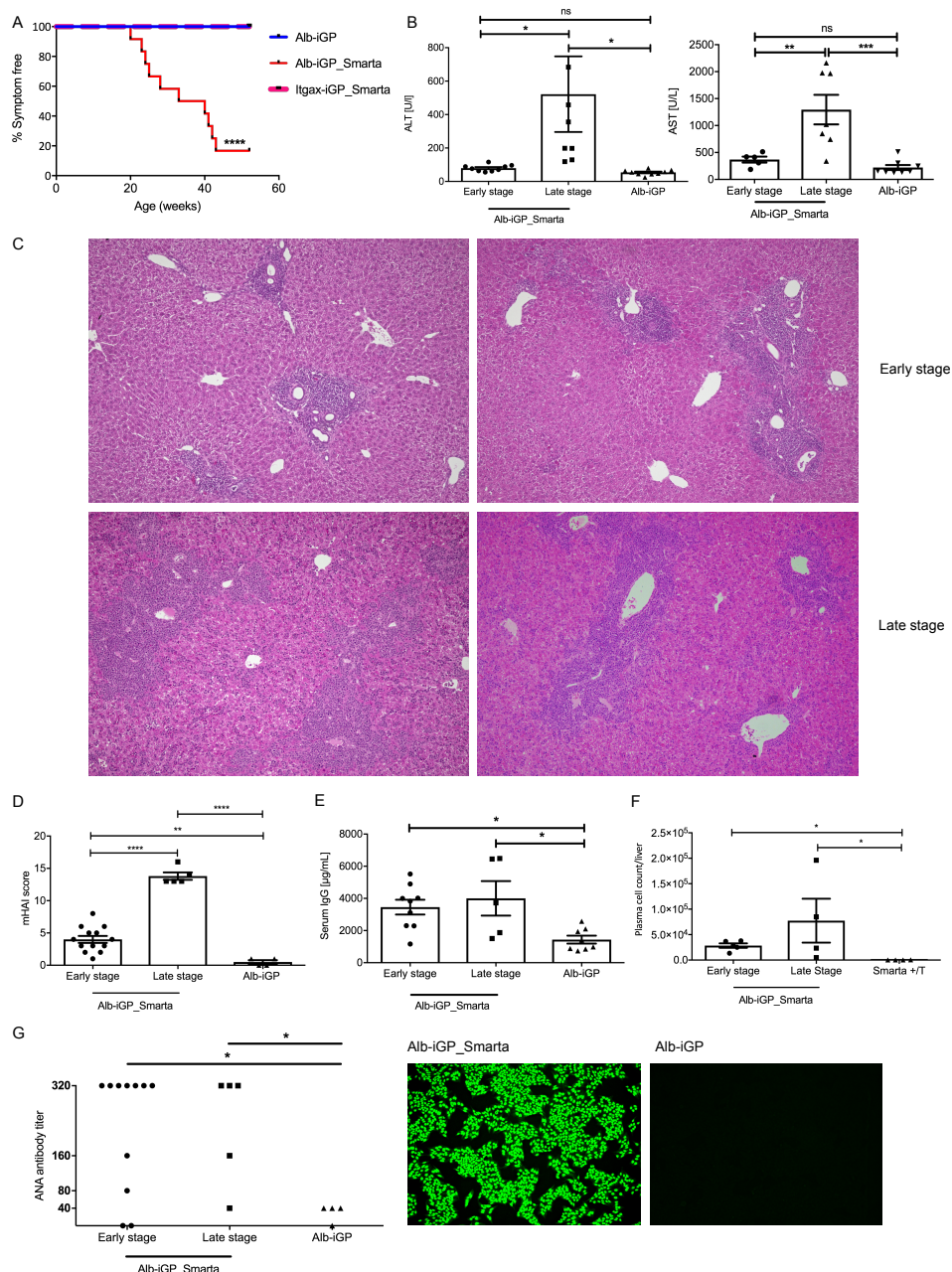


Figure 2: Spontaneous development of AIH features in Alb-iGP_Smartas mice. (A) Spontaneous development of sickness symptoms, shown as age-dependently reduced percentage of symptom-free Alb-iGP_Smartas mice (red line; n=12), compared to Alb-iGP control mice (blue line; n=13) and Itgax-iGP_Smartas control mice (pink line; n=10). (B) Serum ALT and AST (each U/l; n=8-9) in Alb-iGP_Smartas mice at early or late disease stage, and Alb-iGP control mice. (C) Representative histology of two Alb-iGP_Smartas livers in early disease stage, showing periportal infiltrates (upper panels), or late disease stage (lower panels), showing periportal and interface hepatitis with mainly lymphocytic infiltrates. (D) The mHAI score (n=4-13) of Alb-iGP_Smartas livers (early and late disease) and Alb-iGP

control livers. (E) Serum IgG levels (μ g/ml; n=5-9). (F) Hepatic CD19+ CD138+ plasma cells (n=4-5). (G) Antinuclear antibody (ANA) titres (left, n = 4-11) and representative fluorographs (right). Shown are mean and SEM. ****p<0.0001; ***p<0.001; **p<0.01; *p<0.05 (A: Mantel-Cox; B,D,E: ANOVA; F: Fisher's exact test).

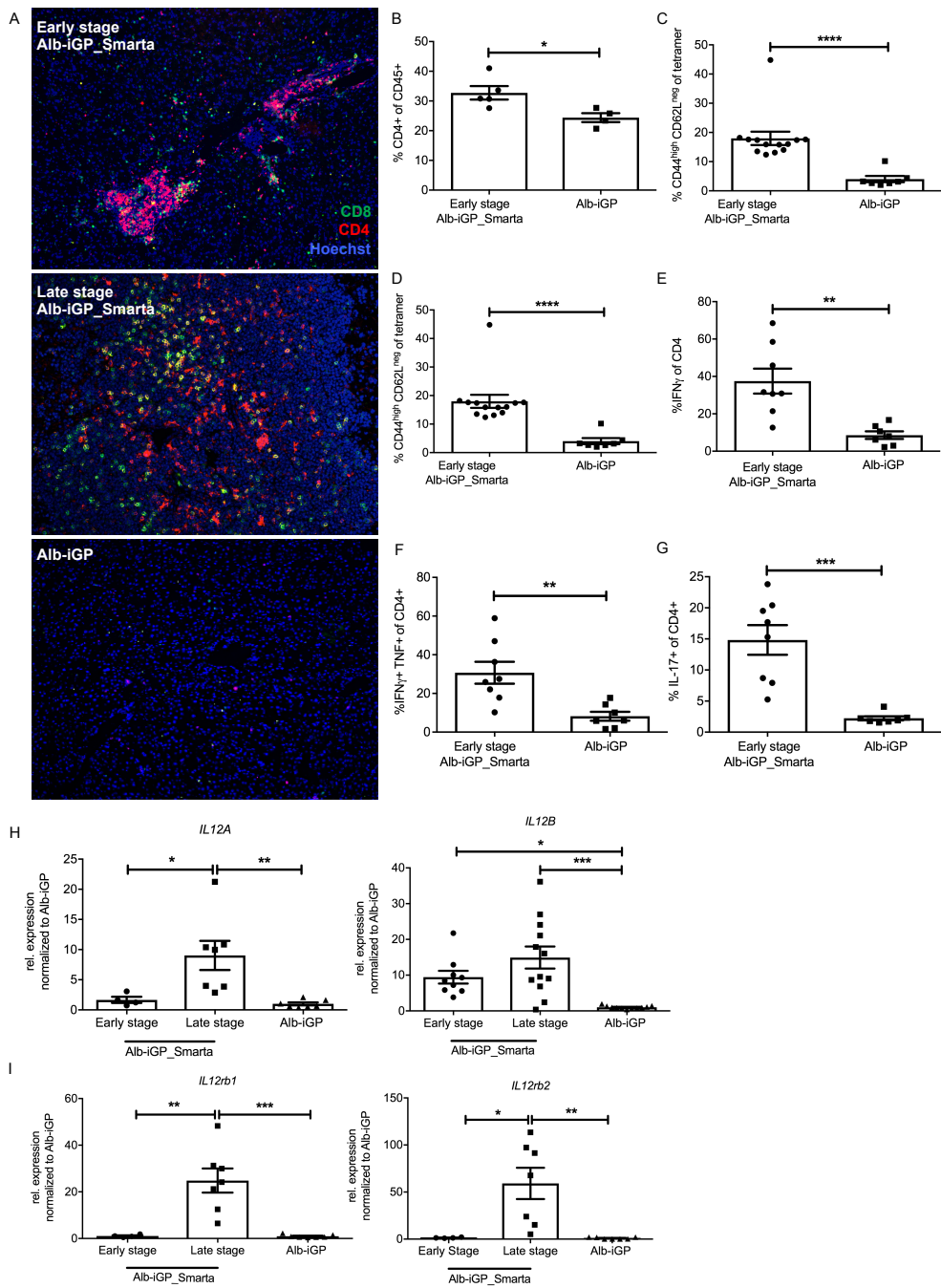


Figure 3: Characterization of liver-infiltrating T cells in Alb-iGP_Smarta mice. (A) Immunofluorescence of liver sections revealing infiltration of CD4 (red) and CD8 cells (green) in Alb-iGP_Smarta (upper panel: early stage; middle: late stage) or Alb-iGP control mice (lower panel). Nuclei are stained in blue. **(B)** Percentage of liver-infiltrating CD4 T cells in Alb-iGP Smarta and Alb-iGP control mice (n=4-5). **(C)** Percentage of GP tetramer-binding CD4 T cells in livers of Alb-iGP_Smarta and Alb-iGP control mice (n=4-5). **(D)** Percentage of liver-infiltrating CD4 T cells with activated/memory phenotype in Alb-iGP_Smarta and Smarta

control mice (n=7-13). (E) Frequencies of IFN γ -producing CD4 T cells, (F) TNF and IFN γ co-producing CD4 T cells and (G) IL-17-producing CD4 T cells in livers of Alb-iGP_Smarta and Alb-iGP control mice (n=4-8). (H) Hepatic gene expression of *IL12A* (left), *IL12B* (right), and (I) *IL12rb1* (left) and *IL12rb2* (right) in Alb-iGP_Smarta mice in early or late stage and Alb-iGP control mice (n=4-12). Shown are means and SEM. ****p<0.0001; ***p<0.001; **p<0.01; *p<0.05 (B-E: Mann-Whitney; F-I: ANOVA).

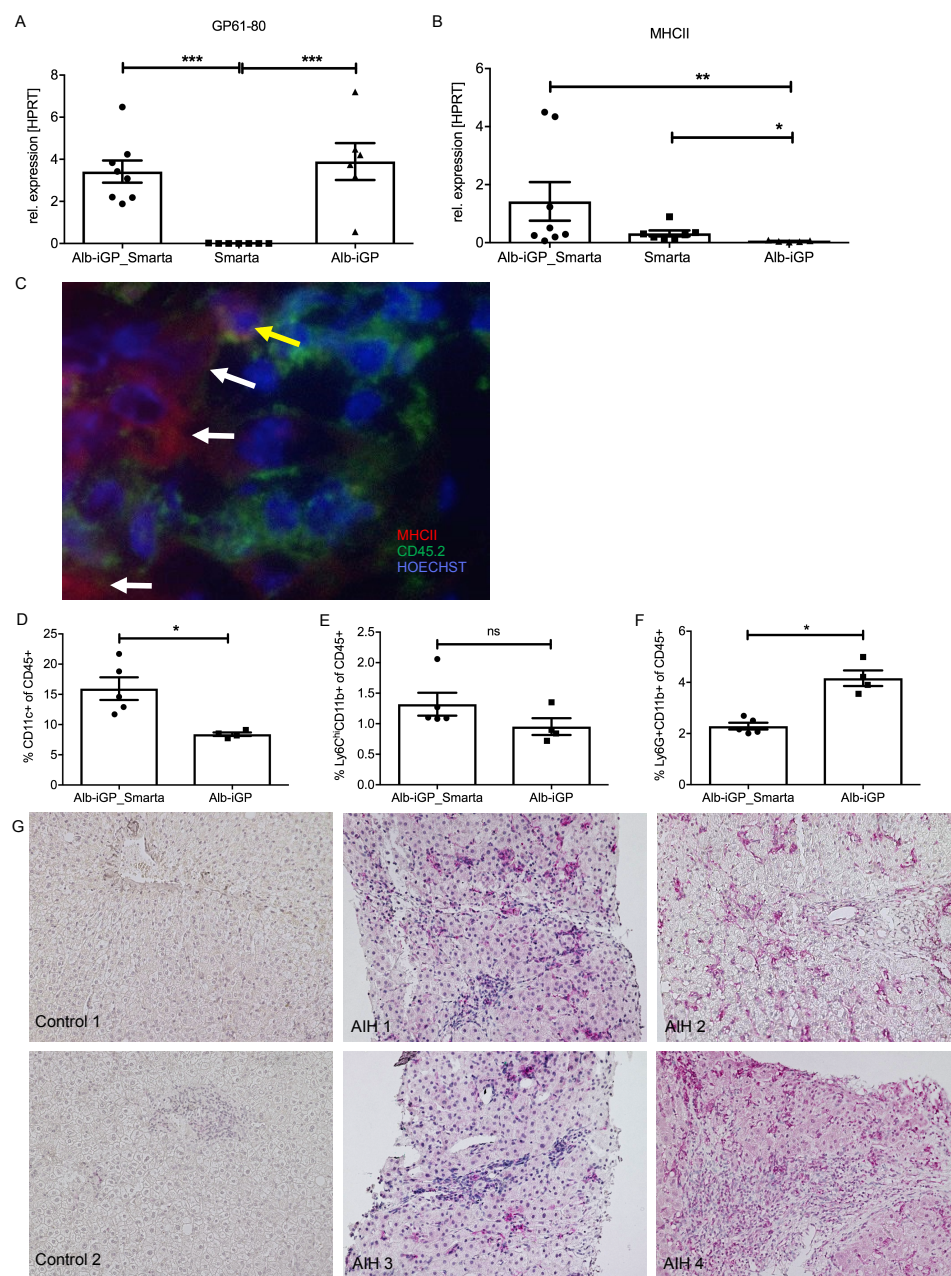


Figure 4: Dendritic cells as pathogenic drivers in Alb-iGP_Smarta mice and human AIH.

Hepatic gene expression of GP (A) and I-A^b (B) in Alb-iGP_Smarta, Smarta, and Alb-iGP mice (n=6-8). (C) Immunostaining of MHCII (red) and CD45 (green) in livers of Alb-iGP Smarta mice. Nuclei are stained in blue. The yellow arrow indicates a CD45+MHCII+ APC, the white arrows indicate CD45-MHCII+ hepatocytes. (D) CD11c+ DCs, (E) Ly6C^{hi}CD11b+ monocytes, (F) Ly6G+CD11b+ neutrophils in livers of Alb-iGP Smarta mice at early stage as compared to Alb-iGP controls. (G) Histological analysis of liver biopsies from newly diagnosed, untreated AIH patients, as compared to pseudo-healthy control tissue from

subjects undergoing bariatric surgery. CD11c positive DCs are stained in pink. Shown are means and SEM. ***p<0.001; **p<0.01; *p<0.05 (A,B: ANOVA; D-H: Mann-Whitney).

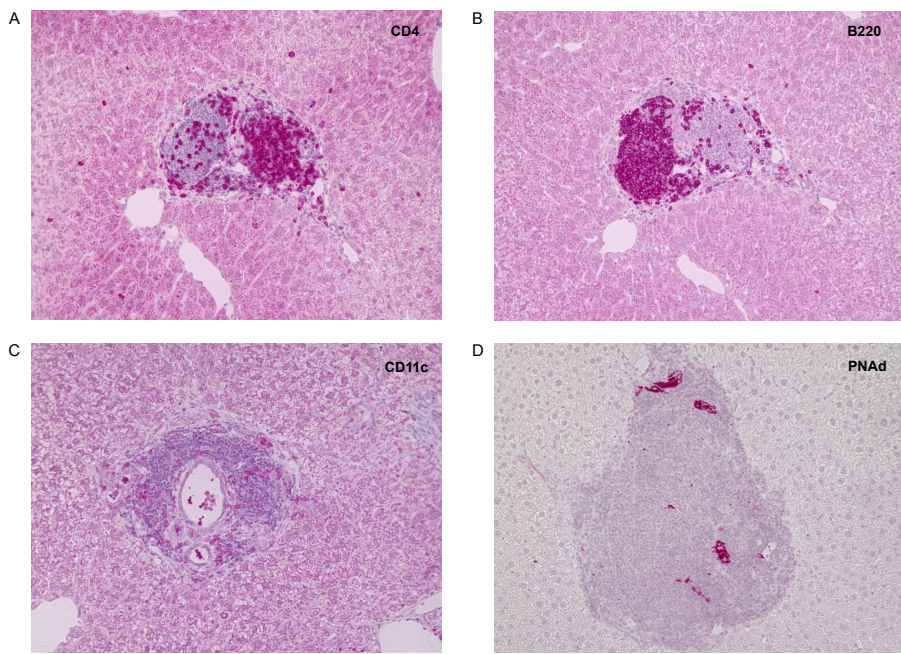


Figure 5: Histological characterization of portal ectopic lymphoid tissue in early disease livers of Alb-iGP_Smarta mice. Segregation of CD4+ T cells (A) and B220+ B cells (B) in separate periportal zones in consecutive sections of Alb-iGP_Smarta livers. (C) CD11c+ dendritic cell network in periportal infiltrate of Alb-iGP_Smarta liver. (D) PNAd+ high endothelial venules in periportal infiltrate of Alb-iGP_Smarta liver.

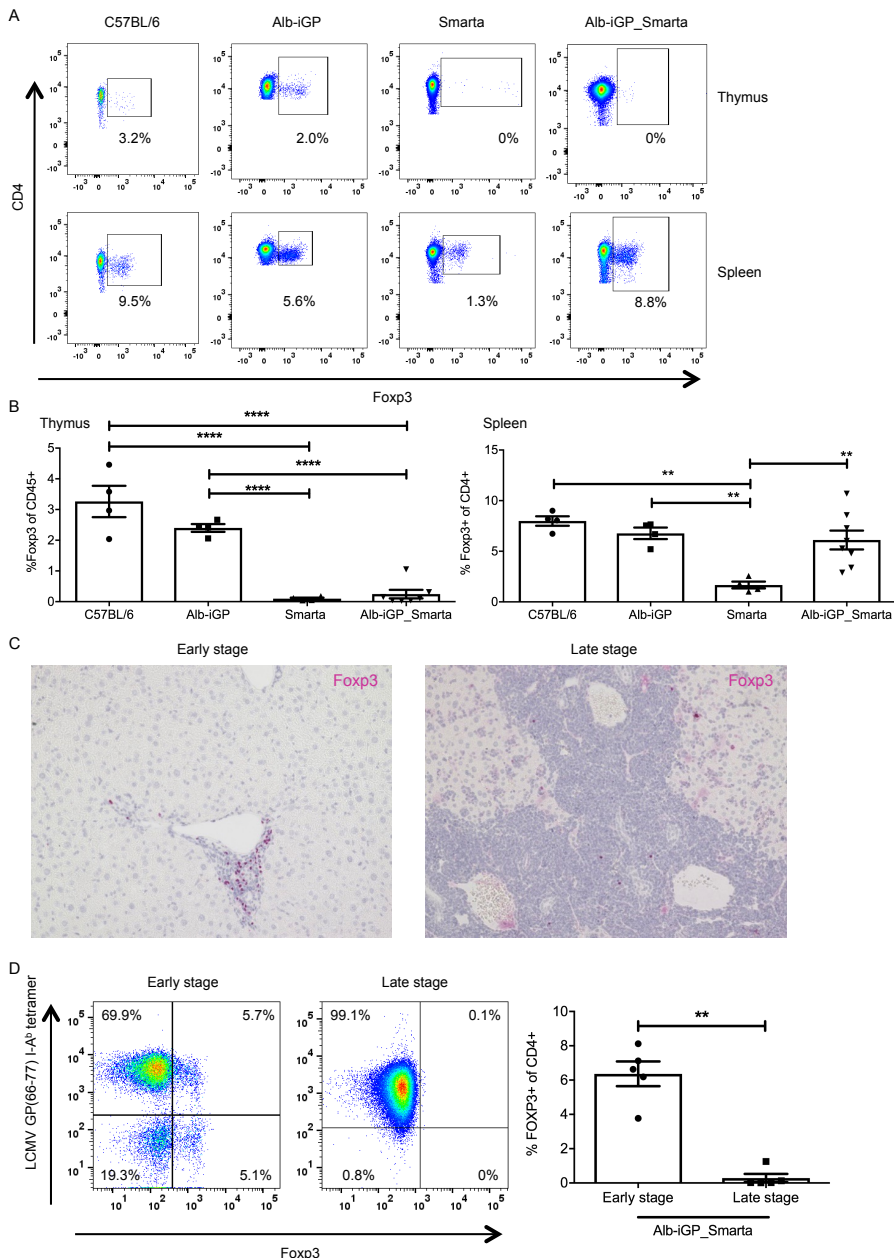


Figure 6: Quantification of regulatory T cells in Alb-iGP_Smarta mice. (A)

Representative flow cytometry dot plots of thymic and splenic Foxp3+ Tregs in C57BL/6, Alb-iGP, Smarta and Alb-iGP_Smarta mice. (B) Frequencies of thymic (left) and splenic (right) CD4+Foxp3+ Tregs in the respective mouse strains (n=4-8). (C) Representative Foxp3 immunohistochemistry of Tregs in periportal infiltrates of Alb-iGP_Smarta liver in early disease (left) or late disease (right). (D) Flow cytometry of antigen-specific (Tetramer+) and non-specific (Tetramer-) CD4+ Foxp3+ Tregs in Alb-iGP_Smarta liver in early disease (left) or late disease (right), and quantification of Treg numbers in early and late stage (n=5).

Shown are mean and SEM. ****p<0.0001; ***p<0.001; **p<0.01; *p<0.05 (B: ANOVA; D: Mann-Whitney).

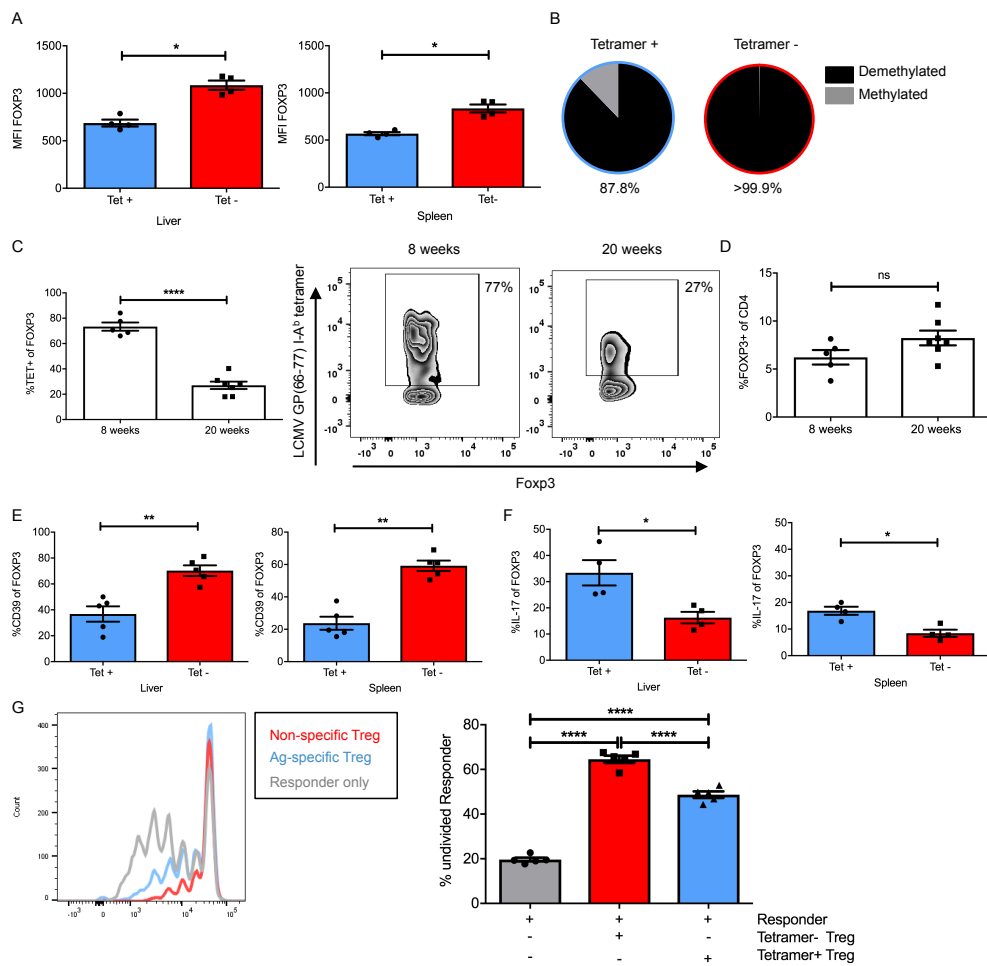


Figure 7: Functional characterization of regulatory T cells in Alb-iGP_Smart mice. (A)

Selectively reduced Foxp3 MFI in tetramer-specific vs. non-specific CD4+ Foxp3+ Tregs in liver and spleen of Alb-iGP_Smart mice (n=4). (B) Reduced CNS2 element demethylation at the Foxp3 gene locus in tetramer-specific vs. non-specific splenic CD4+ Foxp3+ Tregs purified and pooled from 10 Alb-iGP_Smart mice. (C) Age-dependent decline of tetramer-specific vs. non-specific CD4+ Foxp3+ Tregs (n=5-7). (D) No age-dependent change in overall Foxp3+ Treg frequency among CD4+ T cells (n=5-7). (E) Selectively reduced percentage of CD39-expressing cells, and (F) selectively increased percentage of IL-17 producers among tetramer-specific vs. non-specific CD4+ Foxp3+ Tregs in liver and spleen of Alb-iGP_Smart mice (n=4). (G) Selectively reduced suppressive function of tetramer-specific (blue) vs. non-specific (red) splenic CD4+ Foxp3+ Tregs of Alb-iGP_Smart mice (n=5). Shown are means and SEM. ****p<0.0001; ***p<0.001; **p<0.01 (A,C,D: Mann-Whitney; E: ANOVA).

Table 1: Penetrance of AIH features in younger and older Alb-iGP_Smart mice (n=10-13)

Disease feature	Penetrance in preclinical phase Early stage (4-20 weeks of age)	Penetrance in disease
		Late stage (>20 weeks of age)
Portal infiltration	100%	100%
Portal ELT	80%	0%
Interface hepatitis	0%	85%
Autoantibodies	80%	80%
IgG elevation	66%	60%
ALT elevation	11%	100%

Table 2: Characteristics of patients included in histological staining in Fig.4G

Patients	Sex (m/f)	Age	ALT	AST	IgG	Disease status
AIH1	m	22	338	721	20.6	acute therapy-naïve AIH
AIH2	m	41	141	87	19.5	acute therapy-naïve AIH
AIH3	f	79	788	367	74.7	acute therapy-naïve AIH
AIH4	f	51	748	1247	25.8	acute therapy-naïve AIH
Control1	f	47	59	71	n.d.	subjected to bariatric surgery
Control2	f	38	47	51	n.d.	subjected to bariatric surgery